
Breaking the Simplification Bottleneck in Amortized Neural Symbolic Regression

Paul Saegert¹ Ullrich Köthe¹

Abstract

Symbolic regression (SR) aims to discover interpretable analytical expressions that accurately describe observed data. Amortized SR promises to be much more efficient than the predominant genetic programming SR methods, but currently struggles to scale to realistic scientific complexity. We find that a key obstacle is the lack of a fast reduction of equivalent expressions to a concise normalized form. Amortized SR has addressed this by general-purpose Computer Algebra Systems (CAS) like SymPy, but the high computational cost severely limits training and inference speed. We propose **SimpliPy**, a rule-based simplification engine achieving a 100-fold speed-up over SymPy at comparable quality. This enables substantial improvements in amortized SR, including scalability to much larger training sets, more efficient use of the per-expression token budget, and systematic training set decontamination with respect to equivalent test expressions. We demonstrate these advantages in our **Flash-ANSR** framework, which achieves much better accuracy than amortized baselines (NeSymReS, E2E) on the FastSRB benchmark. Moreover, it performs on par with state-of-the-art direct optimization (PySR) while recovering more concise instead of more complex expressions with increasing inference budget.

1. Introduction

Symbolic regression (SR) occupies a unique position in scientific machine learning by enabling the discovery of interpretable, closed-form laws from observational data (Schmidt & Lipson, 2009). Unlike standard deep learning, SR seeks the analytical expressions that govern the data-generating process. Traditionally, this is framed as a combinatorial optimization problem solved via genetic programming (GP)

¹Computer Vision and Learning Lab, Heidelberg University, Germany. Correspondence to: Paul Saegert <bc226@uni-heidelberg.de>, Ullrich Köthe <ullrich.koethe@iwr.uni-heidelberg.de>.

(Koza, 1994; Cranmer, 2023). While GP remains the gold standard for precision, it treats every dataset as a *tabula rasa* search instance, failing to transfer structural knowledge between tasks and acquire experience.

Pioneered by Lample & Charton (2019); Biggio et al. (2021), amortized SR solves this by learning the posterior $p(\text{expression}|\text{data})$ over millions of examples, aiming to shift the computational burden to a one-time pre-training phase. Meanwhile, neural scaling laws dictate that robust generalization requires vast and diverse (Kaplan et al., 2020), and high quality (Lample & Charton, 2019; Lee et al., 2022; Gunasekar et al., 2023) data. This presents a fundamental challenge: randomly generated mathematical expressions are rife with redundancies (e.g., $x + x$ vs. $2x$) that must be *simplified* to ensure high-quality, normalized training targets.

Current state-of-the-art approaches face a dilemma regarding this simplification step. Standard Computer Algebra Systems (CAS) like SymPy (Meurer et al., 2017) rely on heavy object-oriented parsing and tree traversals. When integrated into training loops (Bendinelli et al., 2023; Yu et al., 2025), this creates a *simplification bottleneck*, where data generation becomes orders of magnitude slower than gradient updates. To maintain feasible training times, many compromise on the amount or diversity of the training data, or abandon simplification entirely (Kamienny et al., 2022).

We introduce SIMPLIPY¹, an engine that reduces symbolic simplification to fast pattern matching, achieving speedups of up to 100× over SymPy at comparable quality. This breakthrough enables FLASH-ANSR² (Figure 1), a framework for Transformer-based training on a continuously generated stream of high-quality expressions. Freed from the common CAS bottleneck, FLASH-ANSR can be scaled to learn to approximate the posterior over a much broader distributions of mathematical functions and data.

Contributions:

1. We identify the simplification bottleneck as a key obstacle to scaling the training and inference of amortized SR and introduce SIMPLIPY, a hash-based simplifica-

¹<https://github.com/psaegert/simplipy>

²<https://github.com/psaegert/flash-ansr>

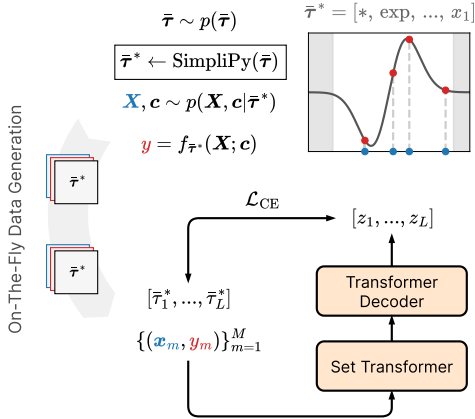


Figure 1. The FLASH-ANSR training pipeline. Following the established standard encoder-decoder paradigm, our framework integrates **SimpliPy** (top center) into the loop for synchronous simplification of on-the-fly generated training expressions.

tion engine to resolve it.

2. We present FLASH-ANSR, which leverages SIMPLIPY to train on 512M on-the-fly generated and simplified data-expression pairs, scaling to higher-dimensional inputs and broader operator sets than prior work.
3. We demonstrate that FLASH-ANSR dominates the inference-time-recovery-rate Pareto frontier against both static (NeSymReS) and unsimplified (E2E) baselines, and matches state-of-the-art GP methods (PySR) with superior inference-time-parsimony scaling.
4. Addressing the pervasive lack of rigor regarding data leakage and evaluation standards in the field, we implement strict *symbolic and numeric decontamination* of training data, ensuring our results reflect actual generalization. We follow a rigorous *test-time compute* evaluation protocol, exposing the inference time budget trade-offs often obscured in prior literature.

2. Related Work

Symbolic regression (SR) has traditionally been formulated as a combinatorial optimization problem. While genetic programming (GP) approaches like PySR (Cranmer, 2023) and Operon (Burlacu et al., 2020) remain the gold standard for precision, they treat every task as a new search instance. Amortized methods aim to overcome this by learning a parameterized approximation of the posterior distribution $p(\tau|\mathcal{D})$ of expressions τ given tabular data \mathcal{D} over a massive training corpus. However, existing approaches are compromised by the trade-off between expression quality (i.e. simplification), and data diversity and scale.

2.1. Static Corpora and Finite Support

To ensure high-quality training targets, many amortized methods rely on SymPy (Meurer et al., 2017) for simplification. Its computational cost, however, leads many to perform data generation offline, resulting in fixed, pre-computed datasets on the order of 100M expressions (Biggio et al., 2021; Vastl et al., 2024). These expensive and limited training sets ultimately force a trade-off between coverage, diversity, and dimensionality: to maintain a representative density of samples over the prior, training is restricted to limited operator sets and low-dimensional settings ($D \leq 3$). Furthermore, these static datasets are confined to iterating over a fixed subset of the prior, fundamentally restricting the diversity of functional forms the model is exposed to during training compared to on-the-fly expression generation.

2.2. Lack of Normalization and Syntactic Redundancy

To escape the limitations of expensive static datasets, recent works have moved toward on-the-fly procedural generation. However, to maintain training throughput, several methods abandon simplification as a consequence, and train on vast streams of unsimplified expressions (Kamienny et al., 2022; Li et al., 2025). This forces the model to approximate a redundant one-to-many mapping during training where a single underlying function has infinite valid representations (e.g., x , $x+0$, $1 \cdot x$) which dilutes the probability mass across syntactically distinct but semantically identical targets. This learned *syntactic redundancy* severely hampers inference efficiency. The generative search dissipates its budget producing syntactic rewrites rather than distinct functional hypotheses, and, since they are not filtered, the constants have to be redundantly re-optimized for each variant.

2.3. The SymPy Bottleneck in Dynamic Generation

A third category of methods attempts to combine on-the-fly generation with CAS-based simplification. NSRwH (Bendinelli et al., 2023) and MDLformer (Yu et al., 2025) apply SymPy within the training loop to simplify generated skeletons. This raises the data quality but introduces a severe computational bottleneck for large scale training. The overhead of object-oriented parsing and tree traversals in SymPy restricts the throughput and maximum complexity of expressions that can be generated in real-time. Consequently, these methods are often limited to lower-dimensional problems.

FLASH-ANSR resolves this dilemma via SIMPLIPY, enabling the high-throughput generation of simplified expressions with high dimensionality and broad operator support, significantly exceeding the scale of prior dynamic methods.

2.4. Methodological Deficiencies in Evaluation.

We identify a pervasive lack of rigor in SR concerning data handling and evaluation. Many works report point-estimates without confidence intervals (Bendinelli et al., 2023) or use lenient success thresholds ($R^2 > 0.9$) that mask failures (d’Ascoli et al., 2023). Analyses often ignore inference time budgets, comparing methods with vastly different compute budgets (Valipour et al., 2021). Most alarmingly, we find that with the partial exception of (Biggio et al., 2021) virtually no prior work performs rigorous data decontamination. This risks performance overestimation (Carlini et al., 2023) and violates fundamental evaluation principles (Hastie et al., 2009). Our work establishes a strict evaluation protocol: We demand machine-precision recovery ($FVU < 10^{-7}$), analyze the *test-time compute* Pareto frontier with respect to a diverse set of metrics, and perform rigorous and conservative decontamination to prevent test set leakage.

3. Method

We formally cast symbolic regression as a set-to-sequence task. \mathcal{S} is our set of mathematical *symbols*: variables $\mathcal{V} = \{x_1, \dots, x_D\}$, operators $\mathcal{O} \in \{+, -, *, /, \text{pow}, \text{sin}, \dots\}$ and \diamond as a placeholder for constants. Very common sub-expressions like `pow2` and `div3` are abbreviated by specialized symbols. We represent a mathematical expression as a sequence of *tokens* $\tau = (\tau_1, \dots, \tau_L)$, where each token represents a single symbol in pre-order notation, see Appendix H for details. Our goal is to learn the posterior $p(\tau|\mathcal{D})$, mapping observed datasets $\mathcal{D} = \{(\mathbf{x}_m \in \mathbb{R}^D, y_m \in \mathbb{R})\}_{m=1}^M$ to plausible (i.e. high probability) generating expressions τ .

Our framework relies on three synergistic components: (1) SIMPLIFY, a novel pattern-matching engine that reduces algebraic simplification to efficient lookups and cancellations; (2) a synchronous, high-throughput data generation pipeline that leverages SIMPLIFY to produce a vast stream of simplified training samples; and (3) a specialized encoder-decoder Transformer architecture.

3.1. SimpliPy: Amortized Symbolic Simplification

To enable high-throughput generation of concise expressions, we introduce SIMPLIFY. It reduces complex expressions to equivalent normalized forms: $s(\tau) \rightarrow \tau^*$. Standard computer algebra solves this problem from first principles, but this is overkill for the kind of expressions encountered in SR training and therefore unnecessarily slow. Instead, we apply an *amortization* strategy to the simplification process itself and determine normalized forms for (sub)expressions with up to four variables and seven symbols offline up-front. This one-time investment allows us to reduce runtime simplification to fast table lookups.

SIMPLIFY operates directly on the tokenized prefix se-

quence produced by the generator and consumed by the model, allowing us to bypass additional parsing overhead caused by conversions to object-oriented structures.

Phase 1: Amortized Rule Discovery (Offline). We employ a variation of Kruskal’s algorithm (Kruskal, 1956) to find a partial, heuristically bounded directed minimum spanning forest over a dynamically generated graph G with expressions as nodes and simplification rules as edges with weight $w(\tau_a, \tau_b) = \max(|\tau_a|, |\tau_b|)$. We consider symbols \mathcal{S}' with $D = 4$ and additional literals $\{0, \pm 1, \pi, e, \pm\infty, \text{NaN}\}$ to allow for informative intermediate representations.

1. **Implicit Sorting:** For each length $L \in \{1, \dots, L_{\max}\}$ in ascending order, we add every prefix expression τ over \mathcal{S}' with $|\tau| = L$ as nodes to the graph G .
2. **Find & Compress:** We attempt to find a node $\tilde{\tau}^* = \text{SIMPLIFY}_{\mathcal{R}}(\tau)$ with the current edges (rules) \mathcal{R} .
3. **Selection:** If no such simplification exists, we test every node τ' of smaller length $j \in \{1, \dots, L - 1\}$ in ascending order satisfying $\text{Vars}(\tau') \subseteq \text{Vars}(\tau)$ for functional equivalence with τ using Algorithm 1.
4. **Pre-Union:** Once all equivalent candidate nodes of length j' have been found, we cache the one with the least amount of constants as a new rule ($\tau \rightarrow \tau'$) into a temporary \mathcal{R}_{new} and skip longer nodes for which $j > j'$.
5. **Union:** After iterating through all edge candidates going out from all nodes of length L , we update the graph with the cached edges: $\mathcal{R} \leftarrow \mathcal{R} \cup \mathcal{R}_{\text{new}}$.

We thus create a Minimum Spanning Forest capturing the least amount of rules needed for expression simplification, minimizing the computational cost of pattern matching.

Phase 2: Online Pattern Matching & Cancellation. At runtime, rules are loaded and sorted into operator-specific buckets keyed by pattern length and root node. Explicit rules (those without variables) are hash-indexed for $O(1)$ lookup while rules with variables are stored as trees for subtree matching. Given a prefix expression, our algorithm first attempts exact replacements considering only the most specific patterns without variables on the current subtree. It then widens the search including patterns with variables and searches pattern buckets from largest to smallest pattern length. If no pattern matches the expression, we simplify children and re-consider simplification of the parent. An optional L_{\max} caps the longest pattern considered, providing control over the trade-off between speed and quality.

Between rule passes, the engine runs a multiplicity-based cancellation pass that merges associative and

commutative clusters (e.g., rewriting $[+, \times 1, \times 1]$ to $[\text{mult} 2, \times 1]$) and cancels inverse pairs.

Both steps are interleaved and repeat alternately until convergence or a small iteration budget is reached. In the final expression, operands of commutative operators are sorted to a canonical order.

As an example, SIMPLIFY simplifies

$$\left| \frac{x_1}{2} \right|^2 + c_1 \cdot e^{-\frac{1}{x_2 - x_2}} + c_2 \longrightarrow c_1 + \left(\frac{x_1}{2} \right)^2 \quad (1)$$

effectively cancelling the exponential term, removing the redundant absolute value, and substituting $c_1 \leftarrow c_1 + c_2$.

3.2. Architecture

FLASH-ANSR builds on an encoder-decoder Transformer architecture inspired by Biggio et al. (2021). We opt for the pre-RMSNorm Transformer decoder architecture (Vaswani et al., 2023; Zhang & Sennrich, 2019; Xiong et al., 2020) with multi-head FlashAttention (Dao, 2023). To encode data sets of variable size, we use a variant of the Set Transformer (Lee et al., 2019) to efficiently encode the input data and use $I = S = 128$ induction and seed points respectively. Inspired by Child et al. (2019); Xiong et al. (2020), and Zhang & Sennrich (2019); Zhang et al. (2022), we introduce the pre-norm paradigm to the Set Transformer architecture. We introduce a masked RMSSetNorm based on Zhang & Sennrich (2019); Zhang et al. (2022) to replace the standard LayerNorm (Ba et al., 2016) or SetNorm (Zhang et al., 2022), allowing us to standardize over the same number of axes as SetNorm while only requiring half the number of statistics and re-scaling parameters, and accounting for padding (see Appendix C for derivation).

As in NeSymReS (Biggio et al., 2021), we preprocess inputs to the Set Transformer by representing each scalar by a multi-hot encoding over a fixed bit representation following the IEEE-754 standard (IEEE, 2008). We use 32 bits instead of just 16 bits to represent each scalar value, leading to an input tensor $\mathbf{Z}^{(0)} \in \mathbb{R}^{N \times M \times 32 \cdot (D+1)}$ with batch size N .

3.3. Data Generation

Training data is generated fully on-the-fly following a multi-step process. For each instance, we sample the desired number of operators of the expression $n_{\text{ops}} \sim p_{\text{ops}}(n_{\text{ops}}) \propto \exp[n_{\text{ops}}^\alpha / \lambda]$ with $\alpha = 0.7$ and $\lambda = 1$ limited to numbers in the range $n_{\text{ops}} \in [0, 17]$. A prefix skeleton is then generated with the Lample & Charton algorithm (Lample & Charton, 2019), creating skeletons with up to 35 symbols. Operators are then sampled and assigned to non-leaf nodes with relative weights 10 for the operators $+$, $-$, $*$ and $/$, and weight 1 for all other operators. The leaf nodes are populated by sampling the number of unique variables to be present

in the skeleton $n_{\text{var}^*} \sim \mathcal{U}(1, \min(n_{\text{leaves}}, D))$ limited by the number of available leaves n_{leaves} or the considered maximum dimensionality D . The set of unique variables is then drawn uniformly without replacement from the union of all variables and the constant placeholder $\mathcal{V}_{\text{sample}^*} \subseteq \mathcal{V} \cup \{\diamond\}$. We then randomly duplicate elements of $\mathcal{V}_{\text{sample}^*}$ until reaching multiset $\mathcal{V}_{\text{sample}}$ with n_{leaves} elements before shuffling and substituting them into the leaf nodes of the skeleton.

Next, the skeletons are simplified with SIMPLIFY ($L_{\text{max}} = 4$) and rejected if the simplification produced non-finite symbols, or if they symbolically or numerically match one of the test skeletons. To that end, we structurally prune all constant nodes from both candidate and test skeletons before computing and comparing their images y_{check} on a fixed input $X_{\text{check}} \sim \mathcal{U}(-10, 10)^{512 \times D}$ using Algorithm 1, effectively excluding whole families of expressions from training. Skeletons are held out from training if all point-wise absolute differences fall within 10^{-4} . Non-numeric values (NaN) in the image are treated as matches, contributing to a conservative decontamination strategy.

In the final step, we sample the number of data points $M \sim \mathcal{U}(1, 1024)$ and their values in each dimension j as $x_{mj} \sim \mathcal{U}(a_j, b_j)$ with $a_j, b_j \sim \mathcal{N}(0, \sigma = 10)$. Each constant present in the expression is sampled independently from $\mathcal{N}(0, \sigma = 5)$, and the expression is compiled and evaluated on X via $y = f_{\bar{\tau}}(X; c)$. If y includes complex, non-finite, or non-numeric elements, all data is re-sampled up to 4 times after which the entire instance is rejected. An illustrative example is provided in Appendix I.

3.4. Training

We minimize the cross-entropy loss over the joint distribution of normalized skeletons and datasets $p(\bar{\tau}^*, \mathcal{D})$:

$$\hat{\theta} = \arg \min_{\theta} \mathbb{E}_{\substack{\bar{\tau} \sim p(\bar{\tau}) \\ \mathcal{D} \sim p(\mathcal{D}|\bar{\tau})}} \left[- \sum_{t=1}^L \log p_{\theta}(\bar{\tau}_t^* | \bar{\tau}_{<t}^*, \mathcal{D}) \right] \quad (2)$$

where p_{θ} is the likelihood assigned by the Transformer decoder at step t , conditioned on the previous tokens $\bar{\tau}_{<t}^*$ and the dataset \mathcal{D} encoded by the Set Transformer. Encoder and decoder are trained jointly and end-to-end. We train four models (3M, 20M, 120M, and 1B parameters) using the hyperparameters listed in Appendix B.

3.5. Inference

We opt for autoregressive softmax sampling to generate candidate skeletons $\bar{\tau} \sim p(\bar{\tau}|\mathcal{D})$ at inference time and encourage diversity by capturing the multi-modal nature of the posterior distribution of expressions. Integer multiplication and division operator tokens in $\bar{\tau}$ are replaced with multiplications by free constants at a slightly increased optimization cost to allow for fine-grained numerical optimization of the

expression, e.g. $[..., \text{mult2}, \cdot, \dots] \rightarrow [..., *, \diamond, \cdot, \dots]$. All generated skeletons are then simplified with SimpliPy ($L_{\max} = 4$), deduplicated symbolically, and compiled before their constants are optimized with the Levenberg-Marquardt algorithm (Levenberg, 1944; Marquardt, 1963) under a least-squares objective using SciPy.optimize.curve_fit (Virtanen et al., 2020), yielding optimized expressions $\hat{\tau}$. Optimizations are run in parallel on multiple CPU cores and are restarted 8 times with initial values sampled from $c_0 \sim \mathcal{N}(0, \sigma = 5)$, matching the training prior. Inspired by many other methods (Biggio et al., 2021; Cranmer, 2023), the predicted expressions are then sorted by their fit quality and a parsimony regularization

$$\hat{\tau}^* = \arg \min_{\hat{\tau}} \log_{10} \text{FVU}(\hat{\tau}) + \gamma \cdot |\hat{\tau}| \quad (3)$$

where $\text{FVU}(\hat{\tau})$ is the fraction of variance unexplained (Equation 8) achieved by an expression $\hat{\tau}$, and γ is a small constant penalizing the complexity of a predicted expression. Thus, an expression $\hat{\tau}_b$ is considered better than an expression $\hat{\tau}_a$ if

$$\frac{\text{FVU}(\hat{\tau}_b)}{\text{FVU}(\hat{\tau}_a)} < 10^{-\gamma(|\hat{\tau}_b| - |\hat{\tau}_a|)}. \quad (4)$$

By default, we set $\gamma = 0.05$, meaning that each additional symbol should decrease the FVU by 11% relative to the expression without that symbol.

4. Experiments

We conduct a comprehensive empirical evaluation of FLASH-ANSR against established baselines in amortized SR (NeSymReS, E2E) and direct optimization (PySR) on 115 expressions and data derived from the FASTSRB benchmark (Martinek, 2025)³. Compared to other commonly used benchmarks (e.g. Feynman (Udrescu & Tegmark, 2020), Nguyen (Hoai et al., 2002; Johnson, 2009; Keijzer, 2003; Uy et al., 2011; Petersen et al., 2021)), which restrict the domain of input data to small and arbitrary intervals around zero, FASTSRB adopts the physically motivated data domains of SRSD (Matsubara et al., 2024), ensuring that methods are evaluated on data distributions that reflect real scientific applications.

We evaluate under strict machine-precision recovery metrics and analyze performance as a function of three key scaling axes: test-time compute, data sparsity, and noise robustness.

4.1. Time-Normalized Recovery Rate

We take inspiration from Biggio et al. (2021) and evaluate the inference-time-recovery-rate Pareto frontier by sweeping over a characteristic scaling parameter for each method

³We exclude 5 equations (B4, B7, B17, II.24.17 and III.14.14) due to complications with data sampling

(Table 1), varying the inference time budget from the millisecond regime ($< 0.1\text{s}$) up to a medium-horizon search ($\approx 1000\text{s}$) in powers of 2. No artificial restrictions are imposed on hardware acceleration (see Appendix F), and no model is stopped early during inference. For each test expression, we evaluate on 10 distinctly sampled datasets for short-term runs and 5 for medium-horizon runs. Baselines are configured as close to their default settings as possible (see Appendix G for details).

Table 1. Ranges for characteristic inference-time scaling parameters used to analyze performance across orders of magnitude in inference time. Evaluation of our 1B parameter model (Appendix L) is limited to 64k samples to account for additional inference time induced by the larger model size.

| METHOD | PARAMETER | RANGES | |
|------------|------------|----------------------|----------------------|
| | | Short ($10\times$) | Medium ($5\times$) |
| NeSymReS | Beam Width | 1 ... 32 | 128, 512 |
| E2E | Beam Width | 1 ... 512 | – |
| PySR | Iterations | 1 ... 1024 | 4096, 16k |
| Flash-ANSR | Samples | 1 ... 16k | 64k, 256k |

4.2. Data Sparsity

We evaluate the ability of FLASH-ANSR to recover physical laws from sparse data by varying the number of points to fit, $M \in \{2^0, \dots, 2^{11}\}$. To ensure a fair comparison, we fix the inference budget to approximately 10 seconds per expression for all methods. The specific hyperparameters corresponding to this budget are detailed in Table 2.

Table 2. Fixed test time compute settings for the sparse data and noisy data experiments.

| METHOD | PARAMETER | VALUE |
|-----------------------|------------|-------|
| NeSymReS | Beam Width | 4 |
| E2E | Beam Width | 256 |
| PySR | Iterations | 128 |
| Flash-ANSR v23.0-3M | Samples | 4096 |
| Flash-ANSR v23.0-20M | Samples | 2048 |
| Flash-ANSR v23.0-120M | Samples | 2048 |
| Flash-ANSR v23.0-1B | Samples | 512 |

4.3. Noisy Data

To assess robustness to noise, we introduce additive Gaussian noise to the target variables following a protocol similar to Cava et al. (2021). For the relative noise levels $\eta \in \{10^{-3}, 10^{-2}, 10^{-1}\}$, we corrupt the data via

$$\tilde{y}_m = y_m + \epsilon_m, \quad \epsilon_m \sim \mathcal{N}(0, \sigma = (\eta \cdot \sigma_y)) \quad (5)$$

where σ_y is the standard deviation of the clean targets.

4.4. Metrics

We assess model performance based on two central metrics capturing the goodness of fit and the parsimony of the predicted expressions.

Relying on exact symbolic match criteria for evaluation is fundamentally flawed for two reasons. Incomplete symbolic canonicalizations of functionally equivalent expressions are not identified as such without expensive manual intervention, leading to misleadingly low recovery rates. Purely symbolic criteria also disregard the vast amount of diverse, functionally distinct expressions that can fit the data equally well as the ground truth. Hence, we focus on numeric recovery as the primary criterion for success.

Numeric Recovery Rate (NRR). Since problems can have widely varying output scales, we base our numeric criterion on the Fraction of Variance Unexplained (FVU) between the ground truth values y and the values obtained from a predicted expression \hat{y} . We define the NRR as the percentage of test problems for which the model finds a solution that fits the data up to the machine epsilon for 32-bit floating point numbers, i.e. $FVU(y, \hat{y}) \leq \epsilon_{32} \approx 1.19 \times 10^{-7}$. Furthermore, distinguish between the recovery rate on the fit data split (fNRR) and an unseen validation data split of equal size (vNRR) for each test instance.

Expression Length Ratio. As a proxy for symbolic quality and interpretability, we evaluate the parsimony of the predicted expressions using the ratio of lengths between predicted and ground truth expressions $|\hat{\tau}|/|\tau|$, where $|\tau|$ denotes the number of nodes in the expression tree of τ .

We indicate the objective of each metric, e.g. $NRR \uparrow^{[0,100]}$ and use bootstrapping to estimate the 95% confidence intervals for all statistics (Riezler & Hagmann, 2024).

4.5. Symbolic Simplification Efficiency

We directly compare the effectiveness and efficiency of simplifications with SymPy (Meurer et al., 2017) and SIMPLIFY based on 2^{16} (64k) expressions sampled from our training distribution (Section 3.3). For SymPy, we implement a compatibility layer that converts our tokenized prefix representation to the corresponding infix string. Then, to work around SymPy’s inherent inability to combine symbols representing free constants, we temporarily substitute randomly sampled values $c_k \sim \mathcal{U}(-10, 10)$ into the expression before parsing it with SymPy, measuring the time of its `simplify` routine, and masking numerical values again with the placeholder \diamond . The simplified expression is then converted back to our prefix format with SIMPLIFY’s parse method.

5. Results

5.1. Time-Normalized Recovery Rate

We present the results of the test-time normalized performance on the FASTSRB benchmark in Figure 2.

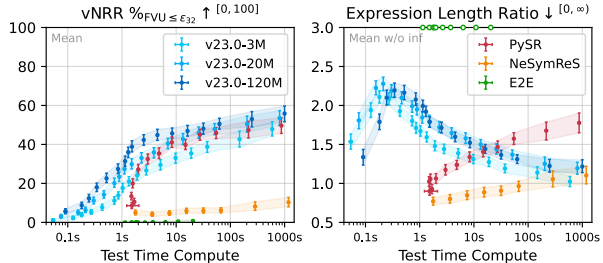


Figure 2. Left: Validation Numeric Recovery Rate (vNRR) as a function of inference time (log scale). FLASH-ANSR models (shades of blue) scale monotonically with compute, with the 120M model partially surpassing the PySR baseline (red). Baselines NeSymReS and E2E fail to generalize to the benchmark. **Right:** Expression Length Ratio $|\hat{\tau}|/|\tau|$ versus compute. We observe a *parsimony inversion*: while PySR increases complexity to minimize error over time, FLASH-ANSR converges toward simpler, more canonical expressions as the sampling budget increases. Shaded regions denote 95% confidence intervals.

Baselines. Consistent with the limitations identified in Section 2, prior amortized methods struggle to generalize to the realistic domains of FASTSRB. NeSymReS saturates at a recovery rate of approximately 10%, while E2E fails to achieve meaningful recovery ($< 2.5\%$) across all budgets.

Accuracy Scaling. FLASH-ANSR demonstrates strong power-law scaling with respect to inference compute. While the smallest model (3M) lags behind the genetic programming baseline, the larger variants and the 1B model (Appendix L) effectively bridge the gap. Notably, the 120M parameter model achieves parity with PySR in the medium-compute regime ($\approx 10s$) and partially surpasses it at higher budgets, reaching a peak recovery rate of 55.8% compared to PySR’s 50.0%. This shows that with sufficient scale and sampling budget, an amortized prior can match or exceed the search efficiency of mature evolutionary algorithms.

The Parsimony Inversion. Crucially, we observe a fundamental divergence in how the methods navigate the accuracy-complexity trade-off (Figure 2, right). PySR employs a sophisticated model selection strategy: it maintains a Pareto front of the best expressions found at every complexity level and selects the final candidate by maximizing the negative gradient of the log-loss with respect to complexity (finding the “knee” of the curve). Without any parsimony penalty beyond this default strategy, however, PySR exhibits a positive correlation between time and expression complexity: as the evolutionary search progresses, the length ratio increases from 0.94 to 1.85. This suggests that even with parsimony pressure, the GP optimizes residual error by ap-

pending corrective terms, resulting in expressions that fit the data via complexity rather than structural discovery.

Conversely, FLASH-ANSR exhibits an *inverse* scaling trend. As the sampling budget increases, the average length ratio of the best-found solution *decreases*, converging towards the ground truth length (e.g., the 120M model improves from 1.40 to 1.27), while simultaneously improving recovery rates. With more compute, the model successfully samples these rarer, concise “needles in the haystack”, rather than constructing complex approximations.

As a realistic application of our method, we present the identification of mathematical test-time scaling laws on the FASTSRB benchmark in Figure 3.

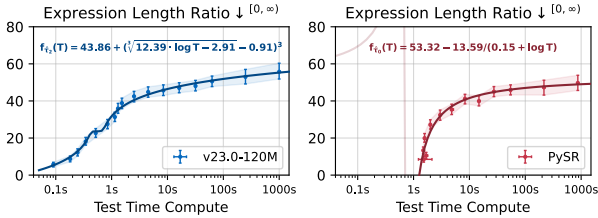


Figure 3. FLASH-ANSR fits to its own and PySR’s scaling curves $\log_{10}(T)$ vs vNRR from Figure 2 (left) using v23.0-120M, $\gamma = 0.15$, 128k choices ≈ 10 min. Extrapolation suggests an asymptotic vNRR $\propto \log T$ scaling for FLASH-ANSR, and an asymptotic upper limit for PySR around 53%.

5.2. Symbolic Simplification Efficiency

Figure 4 characterizes the performance of our SIMPLIFY engine and the SymPy `simplify` routine.

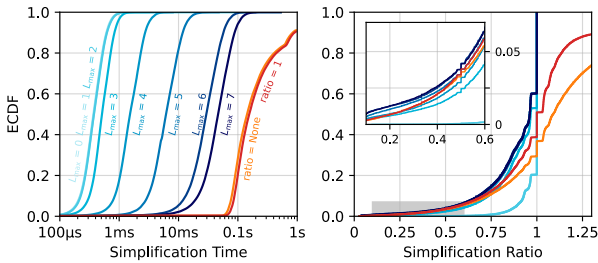


Figure 4. **Left:** Empirical Cumulative Distribution Functions (ECDFs) of simplification wall-clock time. Our SIMPLIFY rewriting engine (shades of blue, varying L_{\max}) operates in the low to moderate millisecond regime, orders of magnitude faster than the SymPy baseline (orange, red). **Right:** ECDF of the simplification ratio $|\tau^*|/|\tau|$. The inset highlights the tail of the distribution. Our method with $L_{\max} \geq 5$ achieves simplification ratios comparable to the SymPy baseline while maintaining high throughput.

Speedup. Our measurements (Figure 4, left) reveal a significant acceleration with respect to the SymPy baseline which exhibits a median simplification time of approximately 100ms per expression, rendering it prohibitive for

real-time applications or large-batch training. In contrast, our pattern-based engine operates in the millisecond regime for $L_{\max} = 4$ (used to train and evaluate FLASH-ANSR).

Quality Preservation. Critically, this speed only comes at a minimal cost of simplification quality. Figure 4 (right) plots the distribution of the simplification ratio $|\tau^*|/|\tau|$. We observe that the distributions for $L_{\max} \geq 5$ even exceed the baseline in terms of conciseness, indicating that our local rewriting rules and cancellations capture the vast majority of reductions found by the more complex heuristics of SymPy. While SIMPLIFY results in strictly shorter or at most equal lengths, SymPy’s simplification paradoxically increases the length of about 38% to 52% of expressions (even with the “ratio” parameter set to 1), and fails to complete within a 1-second timeout for 9% of expressions.

5.3. Data Sparsity

We investigate the impact of data sparsity on model performance by varying the number of support points M from 1 to 2048 (Figure 5). While the amortized baselines (NeSymReS,

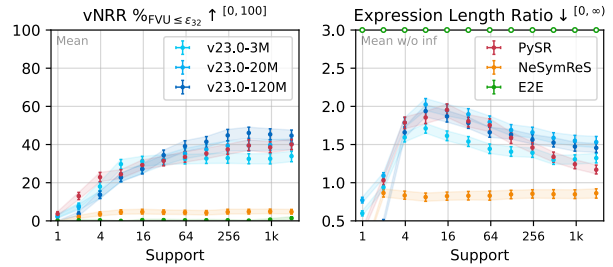


Figure 5. **Left:** Validation Numeric Recovery Rate (vNRR) vs. the number of support points M . FLASH-ANSR (120M) outperforms PySR in the dense data regime ($M > 64$). **Right:** Expression Length Ratio $|\hat{\tau}|/|\tau|$. We observe a distinct “Complexity Peak” at $M \approx 8$, where the model generates expressions significantly longer than the ground truth. This peak coincides with a regime of high uncertainty (low log-probability) and excess constant usage, suggesting the model is *interpolating* the sparse points via complex aliasing rather than identifying the underlying law.

E2E) remain largely ineffective across all regimes, FLASH-ANSR and PySR demonstrate strong scaling behavior.

The structural evolution of the predicted expressions reveals a phase transition analogous to (*Deep*) *Double Descent* (Belkin et al., 2018; Nakkiran et al., 2019). At the critical threshold of $M \approx 8$ points, we observe a “complexity peak” where the average expression length overshoots the ground truth by up to 2 times. This correlates with a surge in excess constants (using degrees of freedom to minimize the fit error) and a dip in the model’s log-probability (Appendix L.2), suggesting a transition through three distinct regimes:

The Parsimonious Regime ($M < 8$): The data is insufficient to contradict the model’s bias toward simplicity and the

scoring function’s preference for parsimonious expressions (Equation 3), resulting in confident, concise approximations with high bias but low variance.

The Interpolation Regime ($M \approx 16$): The data density is sufficient to rule out trivial forms but insufficient to constrain the search to the true symbolic law. To maintain low fit error, the method saturates its complexity budget, inserting excess constants and operators to construct “aliasing” approximations. The drop in log-probability confirms this as a regime of high uncertainty, where probability mass is spread across many complex candidates.

The Identification Regime ($M \rightarrow 2048$): The symbolic cost of explaining the data via complex approximation exceeds the model’s generative capabilities, encouraging a posterior collapse to the ground truth – the only remaining solution that fits the data and is concise enough to be predicted by the model. We observe that distribution shifts in the data can disrupt this delicate balance, preventing successful identification even in the dense data regime.

5.4. Noisy Data

We demonstrate the effects of distribution shifts induced by additive Gaussian noise on the target values in Figure 6.

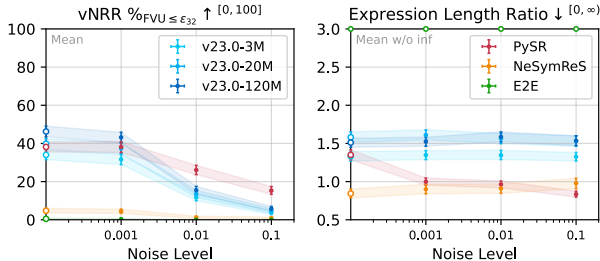


Figure 6. Left: Validation Numeric Recovery Rate (vNRR) vs. the noise level η (log scale). While FLASH-ANSR (shades of blue) achieves competitive performance in the noiseless regime (circles), PySR (red) retains higher recovery rates at larger noise levels. **Right:** Expression Length Ratio $|\hat{\tau}|/|\tau|$. On noisy data, PySR (red) and NeSymReS (orange) produce expressions of similar complexity to the ground truth whereas FLASH-ANSR consistently predicts longer expressions without any apparent trend.

In low-noise settings, FLASH-ANSR demonstrates superior performance with the 120M parameter model surpassing the genetic programming baseline PySR (Figure 6, left). At higher noise levels $\eta \geq 10^{-2}$, we observe a distinct performance crossover. Here, PySR demonstrates better robustness, retaining a higher recovery rate than FLASH-ANSR.

Since FLASH-ANSR was trained exclusively on noiseless data, the injection of noise constitutes a distributional shift. The encoder, having learned that all variance in y carries semantic meaning, misinterprets the noise as high-frequency

signals. Consequently, it attempts to “explain” the noise by continuing to generate expressions with rich functional structures, none of which can perfectly fit the intricate variations induced by the noise (Figure 6, right).

5.5. Training Prior Ablations

Figure 7 highlights the importance of a well-designed training prior. Restricting constant values to a narrow positive range $\mathcal{U}(1, 5)$ as in prior work (Biggio et al., 2021) severely limits the model’s ability to generalize to test expressions with constants near zero or negative values. By expanding the training prior to include negative values and values near zero, the model learns to associate subtle variations in data with corresponding structural changes in the expression, significantly improving recovery rates.

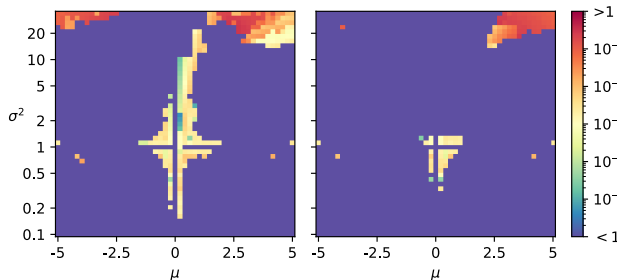


Figure 7. Ablations of FLASH-ANSR fitting a Gaussian function with varying μ and σ . Left: When trained with constants sampled from $\mathcal{U}(1, 5)$ as in prior work (Biggio et al., 2021), the model struggles to correctly identify the function’s shape and constants around the standard values ($\mu = 0, \sigma = 1$). **Right:** Training with a broader prior of $\mathcal{U}(-5, 5)$ improves the ability to recover the correct expression under subtle variations from the standard values.

6. Conclusion

In this work, we introduced SIMPLIFY, a high-throughput simplification engine that breaks a significant bottleneck preventing amortized SR from scaling to scientific complexity. We demonstrate its effectiveness through our FLASH-ANSR framework, which enables large-scale training on diverse and high-quality expressions, and efficient inference.

In our large-scale evaluation on the FASTSRB benchmark, FLASH-ANSR dominates existing amortized baselines and effectively competes with state-of-the-art genetic programming (PySR) on the inference-time vs recovery-rate Pareto frontier in realistic scientific data domains, while recovering more concise expressions as the inference budget increases.

Limitations remain, particularly regarding robustness to noisy data, which acts as an out-of-distribution shift for our models. Future work will focus on further improving the training prior by incorporating noisy data into the training process, widening the range of the generated training data distributions, and exploring alternative encoding and de-

coding paradigms. By establishing rigorous evaluation standards and demonstrating scalable performance, our work positions amortized SR as a powerful, high-speed complement to classical optimization in the toolkit of scientific discovery.

Impact Statement

This paper presents work whose goal is to advance the field of Machine Learning. There are many potential societal consequences of our work, none of which we feel must be specifically highlighted here.

References

- Ansel, J., Yang, E., He, H., Gimelshein, N., Jain, A., Voznesensky, M., Bao, B., Bell, P., Berard, D., Burovski, E., Chauhan, G., Chourdia, A., Constable, W., Desmaison, A., DeVito, Z., Ellison, E., Feng, W., Gong, J., Gschwind, M., Hirsh, B., Huang, S., Kalambarkar, K., Kirsch, L., Lazos, M., Lezcano, M., Liang, Y., Liang, J., Lu, Y., Luk, C., Maher, B., Pan, Y., Puhersch, C., Reso, M., Saroufim, M., Siraichi, M. Y., Suk, H., Suo, M., Tillet, P., Wang, E., Wang, X., Wen, W., Zhang, S., Zhao, X., Zhou, K., Zou, R., Mathews, A., Chanan, G., Wu, P., and Chintala, S. Pytorch 2: Faster machine learning through dynamic python bytecode transformation and graph compilation. In *Proceedings of the 29th ACM International Conference on Architectural Support for Programming Languages and Operating Systems, Volume 2*, pp. 929–947. ACM, 2024. doi: 10.1145/3620665.3640366.
- Ba, J. L., Kiros, J. R., and Hinton, G. E. Layer normalization, 2016. URL <https://arxiv.org/abs/1607.06450>.
- Belkin, M., Hsu, D. J., Ma, S., and Mandal, S. Reconciling modern machine learning and the bias-variance trade-off. *ArXiv*, abs/1812.11118, 2018. URL <https://api.semanticscholar.org/CorpusID:57189215>.
- Bendinelli, T., Biggio, L., and Kamienny, P.-A. Controllable neural symbolic regression, 2023. URL <https://arxiv.org/abs/2304.10336>.
- Biggio, L., Bendinelli, T., Neitz, A., Lucchi, A., and Parascandolo, G. Neural symbolic regression that scales. In *International Conference on Machine Learning*, pp. 936–945. Pmlr, 2021.
- Burlacu, B., Kronberger, G., and Kommenda, M. Operon c++: An efficient genetic programming framework for symbolic regression. In *Proceedings of the 2020 Genetic and Evolutionary Computation Conference Companion*, GECCO ’20, pp. 1562–1570, New York, NY, USA, 2020. Association for Computing Machinery. ISBN 9781450371278. doi: 10.1145/3377929.3398099. URL <https://doi.org/10.1145/3377929.3398099>.
- Carlini, N., Ippolito, D., Jagielski, M., Lee, K., Tramèr, F., and Zhang, C. Quantifying memorization across neural language models. In *The Eleventh International Conference on Learning Representations*, 2023. URL <https://openreview.net/forum?id=P282diP8Cq>.
- Cava, W. L., Orzechowski, P., Burlacu, B., de França, F. O., Virgolin, M., Jin, Y., Kommenda, M., and Moore, J. H. Contemporary symbolic regression methods and their relative performance, 2021. URL <https://arxiv.org/abs/2107.14351>.
- Child, R., Gray, S., Radford, A., and Sutskever, I. Generating long sequences with sparse transformers. *ArXiv*, abs/1904.10509, 2019. URL <https://api.semanticscholar.org/CorpusID:129945531>.
- Cranmer, M. Interpretable machine learning for science with pysr and symbolicregression.jl, 2023. URL <https://arxiv.org/abs/2305.01582>.
- Dao, T. Flashattention-2: Faster attention with better parallelism and work partitioning, 2023. URL <https://arxiv.org/abs/2307.08691>.
- d’Ascoli, S., Becker, S., Mathis, A., Schwaller, P., and Kilbertus, N. Odeformer: Symbolic regression of dynamical systems with transformers. *arXiv preprint arXiv:2310.05573*, 2023.
- Gunasekar, S., Zhang, Y., Aneja, J., Mendes, C. C. T., Giorno, A. D., Gopi, S., Javaheripi, M., Kauffmann, P., de Rosa, G., Saarikivi, O., Salim, A., Shah, S., Behl, H. S., Wang, X., Bubeck, S., Eldan, R., Kalai, A. T., Lee, Y. T., and Li, Y. Textbooks are all you need, 2023. URL <https://arxiv.org/abs/2306.11644>.
- Hägele, A., Bakouch, E., Kosson, A., Allal, L. B., von Werra, L., and Jaggi, M. Scaling laws and compute-optimal training beyond fixed training durations. *ArXiv*, abs/2405.18392, 2024. URL <https://api.semanticscholar.org/CorpusID:270068102>.
- Hastie, T., Tibshirani, R., and Friedman, J. *The Elements of Statistical Learning: Data Mining, Inference, and Prediction*. Springer, New York, NY, 2 edition, 2009.
- Hoai, N. X., McKay, R. I., Essam, D., and Chau, R. Solving the symbolic regression problem with tree-adjunct grammar guided genetic programming: The comparative

- results. In *Proceedings of the 2002 Congress on Evolutionary Computation. CEC'02 (Cat. No. 02TH8600)*, volume 2, pp. 1326–1331. IEEE, 2002.
- Hu, S., Tu, Y., Han, X., He, C., Cui, G., Long, X., Zheng, Z., Fang, Y., Huang, Y., Zhao, W., Zhang, X., Thai, Z. L., Zhang, K., Wang, C., Yao, Y., Zhao, C., Zhou, J., Cai, J., Zhai, Z., Ding, N., Jia, C., Zeng, G., Li, D., Liu, Z., and Sun, M. Minicpm: Unveiling the potential of small language models with scalable training strategies, 2024. URL <https://arxiv.org/abs/2404.06395>.
- IEEE. Ieee standard for floating-point arithmetic. *IEEE Std 754-2008*, pp. 1–70, 2008. doi: 10.1109/IEEESTD.2008.4610935.
- Johnson, C. G. Genetic programming crossover: Does it cross over? In *Genetic Programming: 12th European Conference, EuroGP 2009 Tübingen, Germany, April 15-17, 2009 Proceedings 12*, pp. 97–108. Springer, 2009.
- Kamienny, P.-A., d’Ascoli, S., Lample, G., and Charton, F. End-to-end symbolic regression with transformers, 2022. URL <https://arxiv.org/abs/2204.10532>.
- Kaplan, J., McCandlish, S., Henighan, T., Brown, T. B., Chess, B., Child, R., Gray, S., Radford, A., Wu, J., and Amodei, D. Scaling laws for neural language models, 2020. URL <https://arxiv.org/abs/2001.08361>.
- Keijzer, M. Improving symbolic regression with interval arithmetic and linear scaling. In *European Conference on Genetic Programming*, pp. 70–82. Springer, 2003.
- Koza, J. R. Genetic programming as a means for programming computers by natural selection. *Statistics and Computing*, 4:87–112, 1994. URL <https://api.semanticscholar.org/CorpusID:8750149>.
- Kruskal, J. B. On the shortest spanning subtree of a graph and the traveling salesman problem. *Proceedings of the American Mathematical Society*, 7(1):48–50, 1956. ISSN 00029939, 10886826. URL <http://www.jstor.org/stable/2033241>.
- Lample, G. and Charton, F. Deep learning for symbolic mathematics, 2019. URL <https://arxiv.org/abs/1912.01412>.
- Lee, J., Lee, Y., Kim, J., Kosiorek, A. R., Choi, S., and Teh, Y. W. Set transformer: A framework for attention-based permutation-invariant neural networks, 2019. URL <https://arxiv.org/abs/1810.00825>.
- Lee, K., Ippolito, D., Nystrom, A., Zhang, C., Eck, D., Callison-Burch, C., and Carlini, N. Deduplicating training data makes language models better, 2022. URL <https://arxiv.org/abs/2107.06499>.
- Levenberg, K. A method for the solution of certain non – linear problems in least squares. *Quarterly of Applied Mathematics*, 2:164–168, 1944. URL <https://api.semanticscholar.org/CorpusID:124308544>.
- Li, Y., Liu, J., Wu, M., Yu, L., Li, W., Ning, X., Li, W., Hao, M., Deng, Y., and Wei, S. Mmsr: Symbolic regression is a multi-modal information fusion task. *Information Fusion*, 114:102681, February 2025. ISSN 1566-2535. doi: 10.1016/j.inffus.2024.102681. URL <http://dx.doi.org/10.1016/j.inffus.2024.102681>.
- Loshchilov, I. and Hutter, F. Decoupled weight decay regularization, 2019. URL <https://arxiv.org/abs/1711.05101>.
- Marquardt, D. W. An algorithm for least-squares estimation of nonlinear parameters. *Journal of the Society for Industrial and Applied Mathematics*, 11(2):431–441, 1963. doi: 10.1137/0111030. URL <https://doi.org/10.1137/0111030>.
- Martinek, V. Fast symbolic regression benchmarking, 2025. URL <https://arxiv.org/abs/2508.14481>.
- Matsubara, Y., Chiba, N., Igarashi, R., and Ushiku, Y. Re-thinking symbolic regression datasets and benchmarks for scientific discovery, 2024. URL <https://arxiv.org/abs/2206.10540>.
- Meurer, A., Smith, C. P., Paprocki, M., Čertík, O., Kirpichev, S. B., Rocklin, M., Kumar, A., Ivanov, S., Moore, J. K., Singh, S., Rathnayake, T., Vig, S., Granger, B. E., Muller, R. P., Bonazzi, F., Gupta, H., Vats, S., Johansson, F., Pedregosa, F., Curry, M. J., Terrel, A. R., Roučka, v., Saboo, A., Fernando, I., Kulal, S., Cimrman, R., and Scopatz, A. Sympy: symbolic computing in python. *PeerJ Computer Science*, 3:e103, January 2017. ISSN 2376-5992. doi: 10.7717/peerj-cs.103. URL <https://doi.org/10.7717/peerj-cs.103>.
- Nakkiran, P., Kaplun, G., Bansal, Y., Yang, T., Barak, B., and Sutskever, I. Deep double descent: Where bigger models and more data hurt, 2019. URL <https://arxiv.org/abs/1912.02292>.
- Petersen, B. K., Landajuela, M., Mundhenk, T. N., Santiago, C. P., Kim, S. K., and Kim, J. T. Deep symbolic regression: Recovering mathematical expressions from data via risk-seeking policy gradients. In *Proc. of the International Conference on Learning Representations*, 2021.
- Riezler, S. and Haggmann, M. *Validity, Reliability, and Significance: Empirical Methods for NLP and Data Science*. Synthesis Lectures on Human Language Tech-

- nologies. Springer Cham, 2024. ISBN 978-3-031-57065-0. doi: 10.1007/978-3-031-57065-0. URL <https://doi.org/10.1007/978-3-031-57065-0>.
- Schmidt, M. D. and Lipson, H. Distilling free-form natural laws from experimental data. *Science*, 324:81 – 85, 2009. URL <https://api.semanticscholar.org/CorpusID:7366016>.
- Su, J., Lu, Y., Pan, S., Murtadha, A., Wen, B., and Liu, Y. Roformer: Enhanced transformer with rotary position embedding, 2023. URL <https://arxiv.org/abs/2104.09864>.
- Udrescu, S.-M. and Tegmark, M. Ai feynman: a physics-inspired method for symbolic regression, 2020. URL <https://arxiv.org/abs/1905.11481>.
- Uy, N. Q., Hoai, N. X., O’Neill, M., McKay, R. I., and Galván-López, E. Semantically-based crossover in genetic programming: application to real-valued symbolic regression. *Genetic Programming and Evolvable Machines*, 12:91–119, 2011.
- Valipour, M., You, B., Panju, M., and Ghodsi, A. Symbolicpt: A generative transformer model for symbolic regression. *arXiv preprint arXiv:2106.14131*, 2021.
- Vastl, M., Kulhánek, J., Kubalík, J., Derner, E., and Babuška, R. Symformer: End-to-end symbolic regression using transformer-based architecture. *IEEE Access*, 12:37840–37849, 2024. doi: 10.1109/ACCESS.2024.3374649.
- Vaswani, A., Shazeer, N., Parmar, N., Uszkoreit, J., Jones, L., Gomez, A. N., Kaiser, L., and Polosukhin, I. Attention is all you need, 2023. URL <https://arxiv.org/abs/1706.03762>.
- Virtanen, P., Gommers, R., Oliphant, T. E., Haberland, M., Reddy, T., Cournapeau, D., Burovski, E., Peterson, P., Weckesser, W., Bright, J., van der Walt, S. J., Brett, M., Wilson, J., Millman, K. J., Mayorov, N., Nelson, A. R. J., Jones, E., Kern, R., Larson, E., Carey, C. J., Polat, İ., Feng, Y., Moore, E. W., VanderPlas, J., Laxalde, D., Perktold, J., Cimrman, R., Henriksen, I., Quintero, E. A., Harris, C. R., Archibald, A. M., Ribeiro, A. H., Pedregosa, F., van Mulbregt, P., and SciPy 1.0 Contributors. SciPy 1.0: Fundamental Algorithms for Scientific Computing in Python. *Nature Methods*, 17:261–272, 2020. doi: 10.1038/s41592-019-0686-2.
- Xiong, R., Yang, Y., He, D., Zheng, K., Zheng, S., Xing, C., Zhang, H., Lan, Y., Wang, L., and Liu, T.-Y. On layer normalization in the transformer architecture. *ArXiv*, abs/2002.04745, 2020. URL <https://api.semanticscholar.org/CorpusID:211082816>.
- Yu, Z., Ding, J., Li, Y., and Jin, D. Symbolic regression via mdlformer-guided search: from minimizing prediction error to minimizing description length, 2025. URL <https://arxiv.org/abs/2411.03753>.
- Zhang, B. and Sennrich, R. Root mean square layer normalization. *ArXiv*, abs/1910.07467, 2019. URL <https://api.semanticscholar.org/CorpusID:113405151>.
- Zhang, K. and Shasha, D. Simple fast algorithms for the editing distance between trees and related problems. *SIAM journal on computing*, 18(6):1245–1262, 1989.
- Zhang, L. H., Tozzo, V., Higgins, J. M., and Ranganath, R. Set norm and equivariant skip connections: Putting the deep in deep sets. *Proceedings of machine learning research*, 162:26559–26574, 2022. URL <https://api.semanticscholar.org/CorpusID:250048548>.

A. Examples

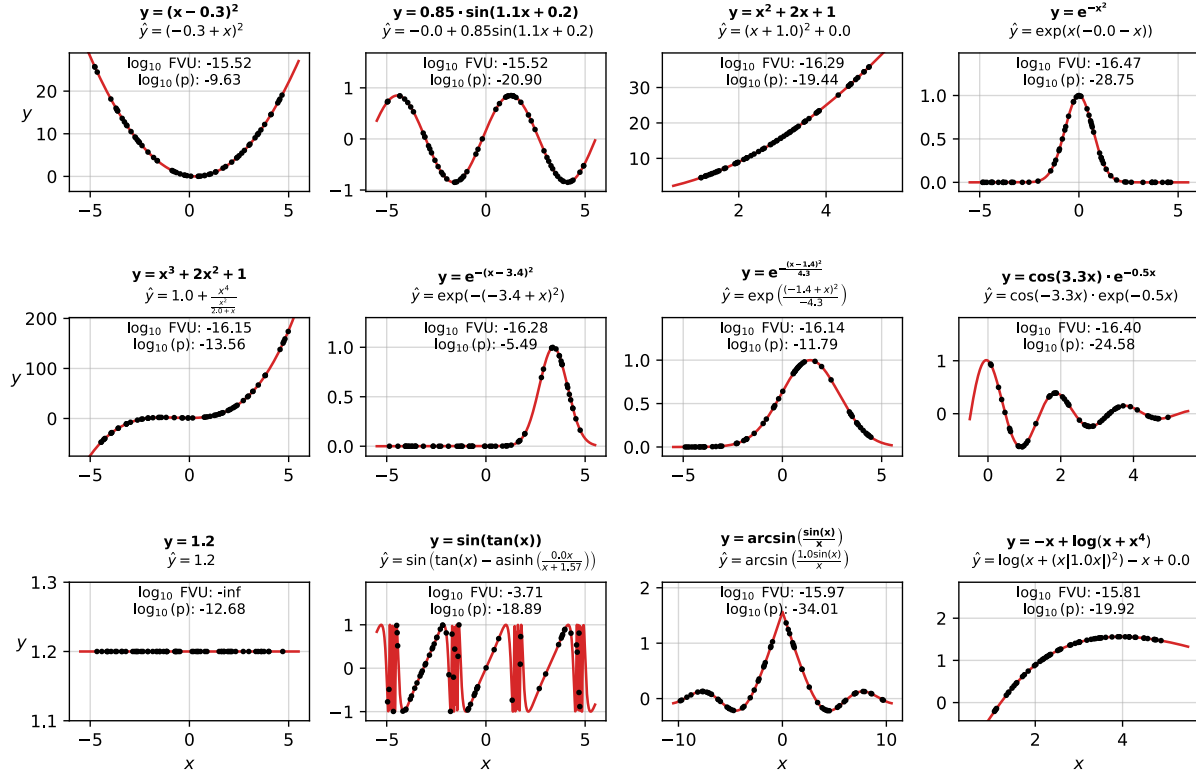


Figure 8. FLASH-ANSR fits (v23.0-120M, $\gamma = 0.05$, 32k samples ≈ 100 s) (red curves) on uniformly sampled data points (black dots) from several 1D expressions ($M = 64$, $\eta = 0$). Many ground truth expressions (bold) are recovered exactly, while others are recovered in alternative forms (e.g. $\hat{y} = (x + 1)^2$ for $y = x^2 + 2x + 1$).

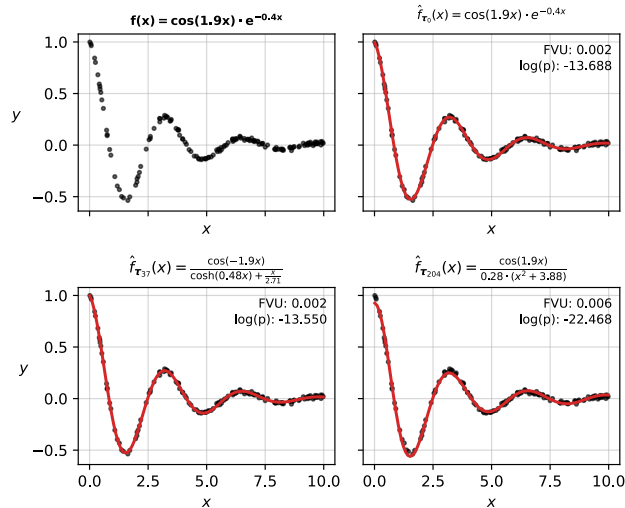


Figure 9. Diverse FLASH-ANSR solutions (v23.0-120M, $\gamma = 0.05$, 32k samples ≈ 100 s) (red curves) on uniformly sampled data points (black dots) depicting the trajectory of a damped harmonic oscillator ($M = 150$, $\eta \approx 0.04$). Multiple distinct expressions fit the data equally well given the noisy data. The ground truth expression (top left, bold) is exactly recovered with high probability (top right). Other solutions (bottom row) achieve similar fit quality while differing structurally.

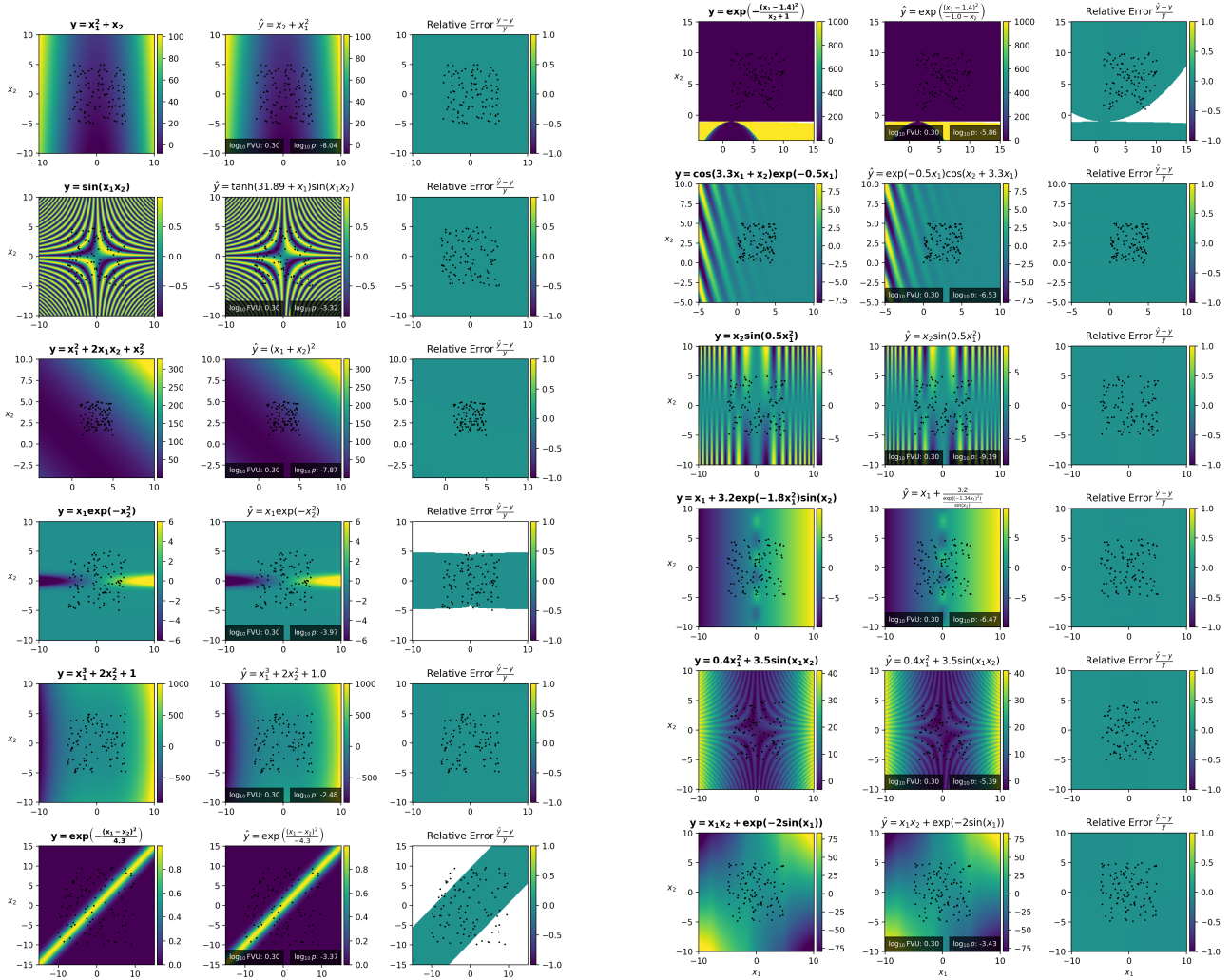


Figure 10. FLASH-ANSR fits (v23.0-120M, $\gamma = 0.05$, 32k samples ≈ 100 s) (middle columns) on uniformly sampled data points (black dots) from several 2D expressions from Biggio et al. (2021) ($M = 100$, $\eta = 0$). Many ground truth expressions (left columns, bold) are recovered exactly, while few others have additional terms that do not affect the relative fit error (right columns)

B. Hyperparameters

We provide a detailed specification of the hyperparameters and training configurations used for the FLASH-ANSR model family to ensure reproducibility below and in Table 3.

Training. All models are trained end-to-end using the AdamW optimizer (Loshchilov & Hutter, 2019) with $\beta_1 = 0.9$. We utilize a Warmup-Stable-Decay learning rate schedule (Hu et al., 2024; Hägele et al., 2024). The learning rate linearly warms up from 0 to a maximum of η_{\max} over the first 10% of optimization steps, remains constant for the subsequent 70% of steps, and follows a linear decay to 0 over the final 20% of steps. We apply gradient clipping with a maximum global norm of 2.0.

Architecture & Implementation. Our models are implemented in PyTorch 2.9. To maximize training throughput on modern GPU architectures, we use Automatic Mixed Precision (AMP) with bf16 precision and `torch.compile` (Ansel et al., 2024). We apply dropout with $p = 0.1$ to the output of Multi-Head Attention blocks and Feed-Forward networks. In the decoder, we utilize Rotary Positional Embeddings (RoPE) (Su et al., 2023) applied to the queries and keys of the self-attention mechanism. The Set Transformer encoder uses $I = 128$ inducing points and $S = 128$ seed vectors across all model sizes.

Table 3. Hyperparameters for the Flash-ANSR model series.

| HYPERPARAMETER | v23.0-3M | v23.0-20M | v23.0-120M | v23.0-1B |
|----------------------------|------------|-----------|------------|-------------------|
| <i>Encoder</i> | | | | |
| Dimension d_{enc} | 192 | 384 | 640 | 1280 |
| Heads | 3 | 6 | 10 | 20 |
| ISAB Layers | 1 | 2 | 5 | 10 |
| SAB Layers | 1 | 2 | 5 | 10 |
| <i>Decoder</i> | | | | |
| Dimension d_{dec} | 192 | 384 | 640 | 1280 |
| Heads | 3 | 6 | 10 | 20 |
| Layers | 3 | 6 | 10 | 20 |
| Feed Forward Dim | 576 | 1152 | 1920 | 3840 |
| <i>Training</i> | | | | |
| Optimizer Steps | 1M | 2M | 3M | 4M |
| Learning Rate η_{max} | 10^{-4} | 10^{-4} | 10^{-4} | $3 \cdot 10^{-5}$ |
| Weight Decay | 0.01 | 0.01 | 0.01 | 0.025 |
| β_2 | 0.95 | 0.95 | 0.95 | 0.99995 |
| Logical CPUs | 4 | 32 | 8 | 8 |
| GPU | RTX 2080Ti | RTX 4090 | A100 | H200 |
| Time Taken | 112h | 56h | 340h | 657h |
| <i>Parameters</i> | | | | |
| Total | 3.2M | 23M | 122M | 955M |
| Encoder | 1.6M | 10.4M | 64.4M | 494M |
| Decoder | 1.6M | 12.4M | 57.5M | 459M |

Simplification. We employ our SIMPLIFY symbolic simplification engine (version dev_7-3) with a maximum pattern length of $L_{max} = 4$ during training and inference.

Ablations. For Figure 7, we use an older version of our model (v7.0 trained with constants sampled from $\mathcal{U}(1, 5)$ and v7.4 trained with constants sampled from $\mathcal{U}(-5, 5)$ but otherwise identical).

C. Masked RMSNorm for Sets

Let $Z \in \mathbb{R}^{N \times M \times d}$ be a tensor representing a batch of N sets, each containing up to M points with dimension d padded with arbitrary values where necessary. Let $\Xi \in \{0, 1\}^{N \times M}$ be a binary mask where $\Xi_{n,m} = 1$ indicates a valid point and 0 indicates padding. We introduce a learnable scaling parameter $\beta \in \mathbb{R}^d$. For each set $n \in \{1, \dots, N\}$, we compute the masked root mean square statistic ν_n over all valid points and features:

$$\nu_n = \sqrt{\frac{\sum_{m=1}^M \sum_{j=1}^d (Z_{n,m,j})^2 \cdot \Xi_{n,m}}{\max(1, d \cdot \sum_{m=1}^M \Xi_{n,m})}} + \epsilon \quad (6)$$

where ϵ is a small constant for numerical stability. The normalized output \hat{Z} is then obtained by scaling the input element-wise:

$$\hat{Z}_{n,m,j} = \frac{Z_{n,m,j}}{\nu_n} \cdot \beta_j \quad (7)$$

D. Model Architecture

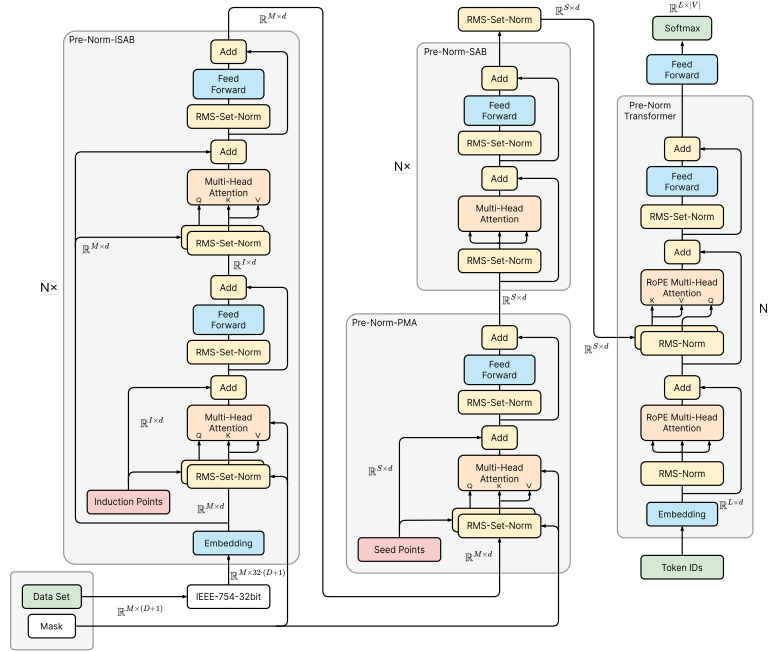


Figure 11. Visual depiction of the Flash-ANSR model architecture. The Set Transformer encoder ingests a variable-sized set of input-output pairs and produces a fixed-size latent representation via Induced Set Attention Blocks (ISAB) and Set Attention Blocks (SAB). The Transformer decoder autoregressively generates a symbolic expression token-by-token, attending to the encoded dataset at each step.

E. Expression Equivalence Checking & SimpliPy Rule Discovery

Algorithm 1 Expression Equivalence Check

```

1: Input: source  $\tau$ , candidate  $\tau'$ , data  $X$ , challenges  $K = 16$ , retries  $R = 16$ 
2: Let  $C$  be constants of  $\tau$ ;  $C'$  be constants of  $\tau'$ 
3: for  $k = 1$  to  $K$  do
4:   Sample  $r \sim \mathcal{N}(0, \sigma = 5)^{|C|}$ 
5:   for  $s \in \{-1, 0, 1\}^{|C|}$  do
6:      $y_\tau \leftarrow f_\tau(X; |r| \odot s)$ 
7:     if  $|C'| = 0$  then
8:       match  $\leftarrow$  allclose( $f_{\tau'}(X), y_\tau$ )
9:     else
10:      match  $\leftarrow$  False
11:      for  $j = 1$  to  $R$  do
12:         $p_0 \sim \mathcal{N}(0, \sigma = 5)^{|C'|}$ 
13:        if  $\exists \hat{c}$  s.t. allclose( $f_{\hat{\tau}}(X; \hat{c}), y_\tau$ ) with Levenberg-Marquardt initialized at  $p_0$  then
14:          match  $\leftarrow$  True; break
15:        end if
16:      end for
17:    end if
18:    if  $\neg$ match then
19:      return False
20:    end if
21:  end for
22: end for
23: return True
    
```

Algorithm 2 SimpliPy Rule Discovery

```

1: Input: Operators  $\mathcal{O}$  (Appendix H), Variables  $\mathcal{V}$ , Literals  $\mathcal{C}$  (Section 3.1), Limits  $L_{\max} = 7, L_{\text{tgt}} = 3$ , Data  $X \sim \mathcal{N}(0, 5)^{1024 \times D}$ , number of challenges  $K = 16$  and retries  $R = 16$ 
2: Initialize rule set  $\mathcal{R} \leftarrow \emptyset$  and pre-compute  $\mathcal{E}_L$ , the set of expressions of length  $L$  using  $\mathcal{O}, \mathcal{V}, \mathcal{C}$  for  $L = 1$  to  $L_{\max}$ 
3: for length  $L = 1$  to  $L_{\max}$  do
4:   Initialize temporary rule cache  $\mathcal{R}_{\text{new}} \leftarrow \emptyset$ 
5:   for each expression  $\tau \in \mathcal{E}_L$  do
6:      $\tau^* \leftarrow \text{SIMPLIPY}_{\mathcal{R}}(\tau)$ ;  $\text{found} \leftarrow \text{False}$ ;  $\tau'_{\text{best}} \leftarrow \text{None}$ 
7:     for length  $j = 1$  to  $\min(|\tau^*| - 1, L_{\text{tgt}})$  do
8:       for each  $\tau' \in \mathcal{E}_j$  where  $\text{Vars}(\tau') \subseteq \text{Vars}(\tau)$  do
9:         if Equivalent( $\tau, \tau'; X, K, R$ ) then
10:          if  $\tau'_{\text{best}} = \text{None}$  or  $|\mathcal{C}(\tau')| < |\mathcal{C}(\tau'_{\text{best}})|$  then
11:             $\tau'_{\text{best}} \leftarrow \tau'$ 
12:          end if
13:           $\text{found} \leftarrow \text{True}$ 
14:        end if
15:      end for
16:      if  $\text{found}$  then
17:         $\mathcal{R}_{\text{new}} \leftarrow \mathcal{R}_{\text{new}} \cup \{\tau \rightarrow \tau'_{\text{best}}\}$ ; break
18:      end if
19:    end for
20:  end for
21:   $\mathcal{R} \leftarrow \mathcal{R} \cup \mathcal{R}_{\text{new}}$ 
22:  Update simplification engine with new rules in  $\mathcal{R}$ 
23: end for
24: return  $\mathcal{R}$ 

```

F. Test-Time Compute System

All runtime-sensitive experiments for Section 5.1 (Time-Normalized Recovery Rate) were conducted on a single representative high-end consumer workstation hardware setup (Table 4) to ensure comparability.

Table 4. System specifications for Time-Normalized Recovery Rate experiment series.

| COMPONENT | SPECIFICATION |
|-----------|------------------------------|
| CPU | AMD Ryzen 9 9950X (16C, 32T) |
| GPU | NVIDIA RTX 4090 (24 GB) |
| RAM | 64 GB DDR5 6000MT/s |
| OS | Ubuntu 24.04.3 LTS |
| Python | 3.13.7 |
| PyTorch | 2.9.1 + CUDA 13.0 |

G. Baselines

Baseline methods are configured at or as close to their defaults as possible while matching the problem setting.

For PySR, we allow the same operator set as FLASH-ANSR, excluding explicit integer multiplication and division operators.

For NeSymReS, we evaluate the “100M” model trained on 100M expressions with the default 4 optimizer restarts.

For E2E, we employ the released `model1.pt` with default refinement parameters (10 trees, 100 bags, 200 points per bag). To attempt evaluation at higher inference budgets (beam width ≥ 512), we apply a dynamic reduction of the maximum generation length to satisfy internal batching constraints. We could not get E2E to function beyond a beam width of 512.

For both, we apply *minimal* compatibility patches to the official implementation to ensure basic functionality in the evaluation

environment. These patches are documented and made publicly available alongside our codebase.

H. Operators

The set of operators supported by FLASH-ANSR and SIMPLIFY is summarized in Table 5. During training, we sample `+`, `-`, `*`, and `/` with weight 10 and all others with weight 1.

Table 5. Flash-ANSR operator vocabulary.

| TOKEN | DESCRIPTION | TOKEN | DESCRIPTION | TOKEN | DESCRIPTION |
|-------------------|----------------|---------------------|---------------|--------------------|-----------------------------|
| <code>+</code> | Addition | <code>pow1_2</code> | \sqrt{x} | <code>asinh</code> | $\operatorname{arcsinh}(x)$ |
| <code>-</code> | Subtraction | <code>pow1_3</code> | $\sqrt[3]{x}$ | <code>acosh</code> | $\operatorname{arccosh}(x)$ |
| <code>*</code> | Multiplication | <code>pow1_4</code> | $\sqrt[4]{x}$ | <code>atanh</code> | $\operatorname{arctanh}(x)$ |
| <code>/</code> | Division | <code>pow1_5</code> | $\sqrt[5]{x}$ | <code>exp</code> | e^x |
| <code>abs</code> | $ x $ | <code>sin</code> | $\sin(x)$ | <code>log</code> | $\log(x)$ |
| <code>inv</code> | $\frac{1}{x}$ | <code>cos</code> | $\cos(x)$ | <code>mult2</code> | $2 \cdot x$ |
| <code>neg</code> | $-x$ | <code>tan</code> | $\tan(x)$ | <code>mult3</code> | $3 \cdot x$ |
| <code>pow</code> | Exponentiation | <code>asin</code> | $\arcsin(x)$ | <code>mult4</code> | $4 \cdot x$ |
| <code>pow2</code> | x^2 | <code>acos</code> | $\arccos(x)$ | <code>mult5</code> | $5 \cdot x$ |
| <code>pow3</code> | x^3 | <code>atan</code> | $\arctan(x)$ | <code>div2</code> | $\frac{x}{2}$ |
| <code>pow4</code> | x^4 | <code>sinh</code> | $\sinh(x)$ | <code>div3</code> | $\frac{x}{3}$ |
| <code>pow5</code> | x^5 | <code>cosh</code> | $\cosh(x)$ | <code>div4</code> | $\frac{x}{4}$ |
| | | <code>tanh</code> | $\tanh(x)$ | <code>div5</code> | $\frac{x}{5}$ |

I. Data Generation Example

We sketch a single draw from our training sampler to illustrate how simplification, test-set guarding, and resampling work.

1) Skeleton draw. We sample $n_{\text{ops}} = 4$ and produce the prefix skeleton with a free constant placeholder \diamond :

$$\bar{\tau}^{(1)} = [+, \text{mult2}, \text{sin}, x_1, \text{pow2}, \diamond].$$

2) Simplification. SimpliPy ($L_{\text{max}} = 4$) absorbs `pow2` into the constant placeholder and simplifies the expression to

$$\bar{\tau}^{(1)*} = [+, \text{mult2}, \text{sin}, x_1, \diamond].$$

3) Test-set guard. We drop constants from both train candidates and held-out expressions, reducing the candidate to

$$\tilde{\tau}^{(1)} = [\text{mult2}, \text{sin}, x_1].$$

Assume the held-out pool contains the expression as its i -th entry

$$\tau_{-}^{(i)} = [\text{mult2}, \text{sin}, /, x_1, \diamond].$$

which reduces to

$$\tilde{\tau}_{-}^{(i)} = [\text{mult2}, \text{sin}, x_1].$$

Since $\tilde{\tau}^{(1)} = \tilde{\tau}_{-}^{(i)}$, we reject this instance and proceed to resampling.

4) Resampling. A new skeleton is drawn with $n_{\text{ops}} = 6$,

$$\bar{\tau}^{(2)} = [*, /, x_1, \text{pow2}, x_2, *, \diamond, +, x_1, \text{neg}, x_1].$$

Simplification yields

$$\bar{\tau}^{(2)*} = [*, /, x_1, \text{pow2}, x_2, \diamond].$$

which, after removing constants, becomes

$$\tilde{\tau}^{(2)} = [/, x_1, \text{pow2}, x_2].$$

No held-out expression matches this skeleton, so we proceed to data sampling.

5) Constant and data draw. The constant is sampled from $\mathcal{N}(0, \sigma = 5)$ as $c_1 = 1.15$. We sample $M = 137$ data points with $X_j \sim \mathcal{U}(a_j, b_j)$ where $a_j, b_j \sim \mathcal{N}(0, \sigma = 10)$. Evaluating $y = f_{\tilde{\tau}^{(2)}}(X; c_1)$ yields finite, real values, so the instance is accepted without further resampling.

J. Data Statistics

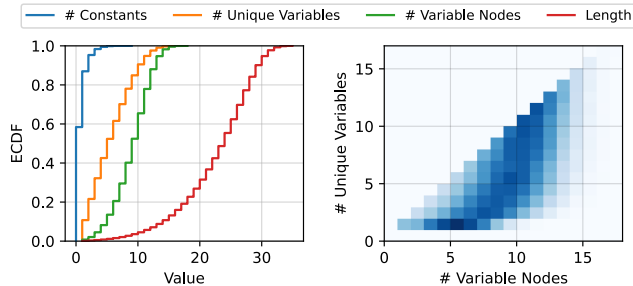


Figure 12. Training data statistics. Left: Empirical Cumulative Distribution Functions (ECDFs) of the number of constants, unique variables, variable nodes and the expression length in the training data. Half of the simplified training expressions contain at least 5 unique variables and 24 symbols. Right: 2D histogram showing the number of unique variables and the number of variable nodes. The training expressions cover both low and high-dimensional regimes with complexity arising both due to the coupling of like and unlike variables.

K. Training Dynamics and Scaling

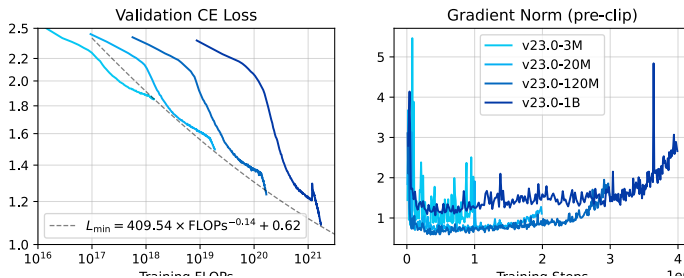


Figure 13. Training dynamics and scaling behavior. **Left:** Validation Cross-Entropy loss (log-scale) as a function of estimated training FLOPs (log-scale) We use the approximation $\text{FLOPs} = 6ND$ following Kaplan et al. (2020), and count FLOPs separately for the encoder with its dataset input and the decoder with its tokenized expression input before adding both for the total FLOPs. The performance envelope generally follows a power-law scaling relationship ($L \propto \text{FLOPs}^{-0.14}$). **Right:** Evolution of gradient norms (pre-clipping). Optimization is stable across the 3M–120M regime. The 1B model exhibits one gradient spike late in training from which it fully recovers over the subsequent training steps. Further investigation is required to determine if this is a systemic issue at large model sizes.

L. Additional Metrics

We use the following definition for the Fraction of Variance Unexplained (FVU):

$$\text{FVU}(y, \hat{y}) = \frac{\sum_{i=1}^N (y_i - \hat{y}_i)^2}{\sum_{i=1}^N (y_i - \bar{y})^2} \quad (8)$$

with $\bar{y} = \frac{1}{N} \sum_{i=1}^N y_i$.

Beyond the primary results, we report the following diagnostics with 95% confidence intervals derived from 1000-fold bootstrapping.

Log₁₀ FVU (non-perfect fits). For cases that are *not* numerically perfect ($\text{FVU} > \epsilon_{32}$), we summarize $\log_{10}(\text{FVU})$. Exact fits are excluded before aggregation.

Numeric Recovery Rate (NRR). For a test set of size K , the fraction of cases where the predicted expression achieves a numerically perfect fit:

$$\text{NRR} = \frac{1}{K} \sum_{k=1}^K \mathbb{I}(\text{FVU}(y^{(k)}, \hat{y}^{(k)}) \leq \epsilon_{32}) \quad (9)$$

with $\epsilon_{32} \approx 1.19 \times 10^{-7}$ being the machine epsilon for 32-bit floating point numbers.

Symbolic Recovery Rate (SRR). Exact structural match between simplified predicted and ground-truth prefix skeletons:

$$\text{SRR} = \frac{1}{K} \sum_{k=1}^K \mathbb{I}(\text{simplify}(\hat{\tau}^{(k)}) = \text{simplify}(\bar{\tau}^{(k)})) \quad (10)$$

Expression F1. Token-level F1 between the predicted prefix skeleton and the simplified ground-truth skeleton.

ZSS Tree Edit Distance. Zhang–Shasha tree edit distance (Zhang & Shasha, 1989) between predicted and ground-truth skeleton trees.

Variable Identification. Recall on the *set of unique variables* present in the simplified predicted vs. ground-truth expressions.

Log Probability. Mean log-probability of the generated sequence under the model.

Excess Constants. Difference in the number of constants between prediction and ground truth. Positive values indicate an overuse of constants to fit the data.

Expression Length Ratio. Length of the predicted prefix skeleton divided by the length of the simplified ground-truth skeleton.

Total Nestedness. Sum of consecutive nestings contributed by unary operators over the predicted expression as a proxy for naturalness and interpretability. For example, $y = \sin(\log(\text{arccosh}(x)))$ has a total nestedness of 2, and $y = \sin(\log(x_1 + \diamond))$ has a total nestedness of 1.

Relative Fit Time. Fit-time multiplier relative to the hyperparameter configuration for the test-time compute experiment.

Fit Success. Fraction of test cases where the fitting procedure completed without errors.

L.1. Detailed Test Time Scaling Results

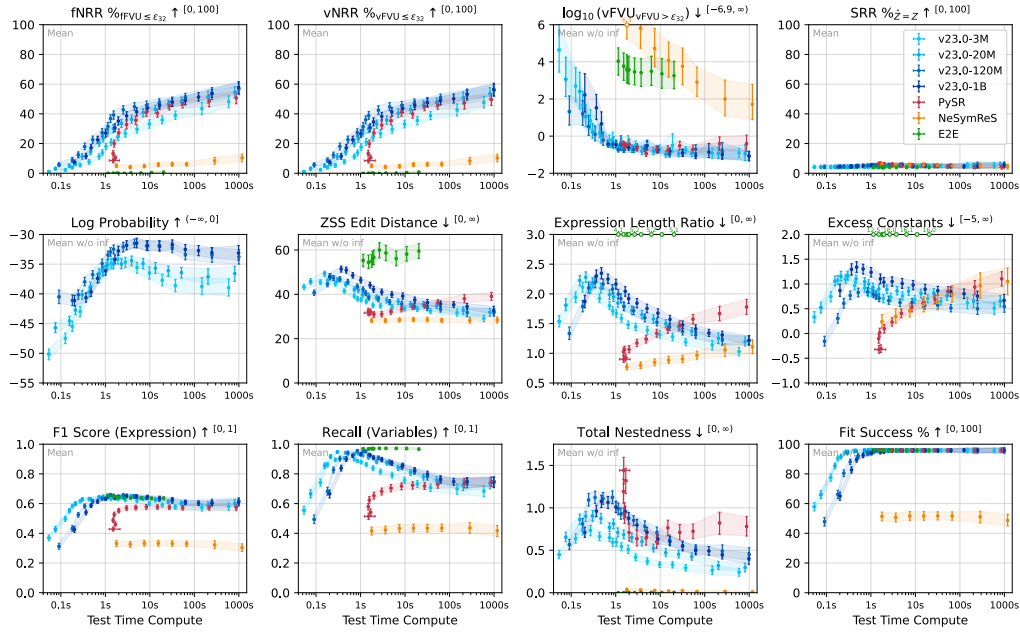


Figure 14. Detailed comparison various time-normalized numerical and symbolic metrics. With increasing time budget, FLASH-ANSR consistently generates more concise (lower expression length ratio), specific (fewer excess constants), and natural (lower total nestedness) expressions than PySR.

L.2. Detailed Data Sparsity Results

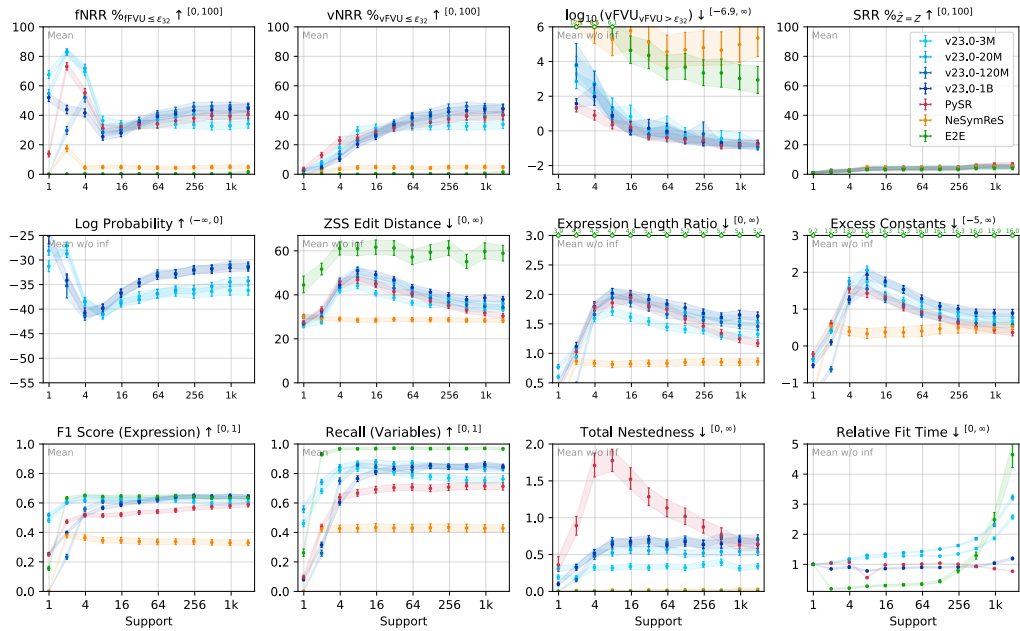


Figure 15. Detailed results for varying number of data points M on the FASTSRB benchmark. In the Interpolation Regime ($N \approx 16$), FLASH-ANSR maintains a lower mean total nestedness than PySR.

L.3. Detailed Noise Level Scaling Results

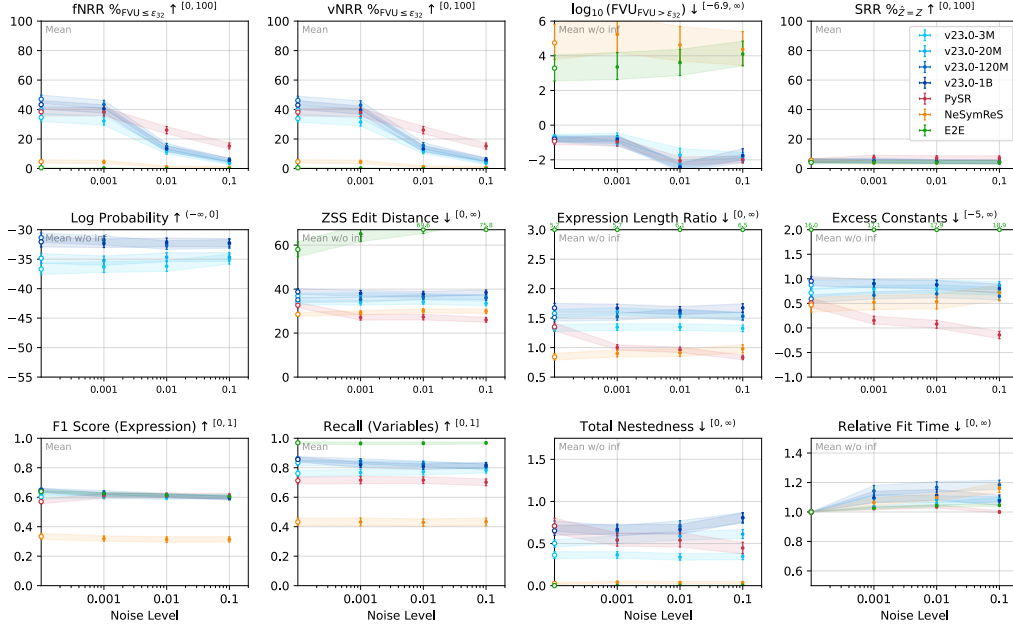


Figure 16. Detailed results for varying noise levels η on the FASTSRB benchmark. Across all noise levels, expressions by FLASH-ANSR maintain similar qualities. With higher noise levels, PySR still achieves shorter and more specific expressions.

M. SimpliPy Rules

Table 6. Random subset of the simplification rules from the SIMPLIFY engine organized into pattern-replacement pairs. The shown expressions are one-dimensional, hence we use x as the variable token. The constant placeholder \diamond represents an arbitrary finite constant. Infinities are carried through the simplification process to enable simplifications such as $\exp(-\frac{1}{x-x}) \xrightarrow{\text{Cancel}} \exp(-\infty) \xrightarrow{\text{Rule 37}} 0$.

| PATTERN | → | REPLACEMENT | PATTERN | → | REPLACEMENT |
|---|---|---------------|---|---|--------------------|
| $(\frac{-\infty}{4})^{\sqrt[3]{\pi}}$ | → | ∞ | $\frac{4x}{\pi}$ | → | $\diamond \cdot x$ |
| $(-\infty)^x \cdot (e \cdot x)$ | → | $(-\infty)^x$ | $(x \cdot \infty) + \frac{x}{\text{NaN}}$ | → | NaN |
| $\frac{1/\pi}{0/(-\infty)}$ | → | ∞ | $\frac{x+(-\infty)}{\sinh(\pi)}$ | → | $-\infty$ |
| $(\infty \cdot 1) \cdot \frac{\pi}{-1}$ | → | $-\infty$ | $\frac{e}{-1} \cdot (-\infty)^\infty$ | → | $-\infty$ |
| $\sinh(\pi)^{x-\infty}$ | → | 0 | $(x \cdot 0)^{-1/e}$ | → | ∞ |
| $\arcsin(0)^{\sqrt[3]{\pi}}$ | → | 0 | $(\pi \cdot \pi) \cdot 2(-\infty)$ | → | $-\infty$ |
| $(-1 - \pi) \cdot (\infty \cdot \pi)$ | → | $-\infty$ | $\sinh(-\infty)^{\arctan(e)}$ | → | ∞ |
| $\frac{x+\infty}{5(-1)}$ | → | $-\infty$ | $(1/2)^{x/3}$ | → | \diamond^x |
| $\frac{\infty^\pi}{\pi+(-1)}$ | → | ∞ | $\arcsin(-1) \cdot \infty^4$ | → | $-\infty$ |
| $\frac{\sqrt{-\infty}}{4\pi}$ | → | ∞ | $(\pi^\pi)^{\infty^3}$ | → | ∞ |

N. Per-Expression Results

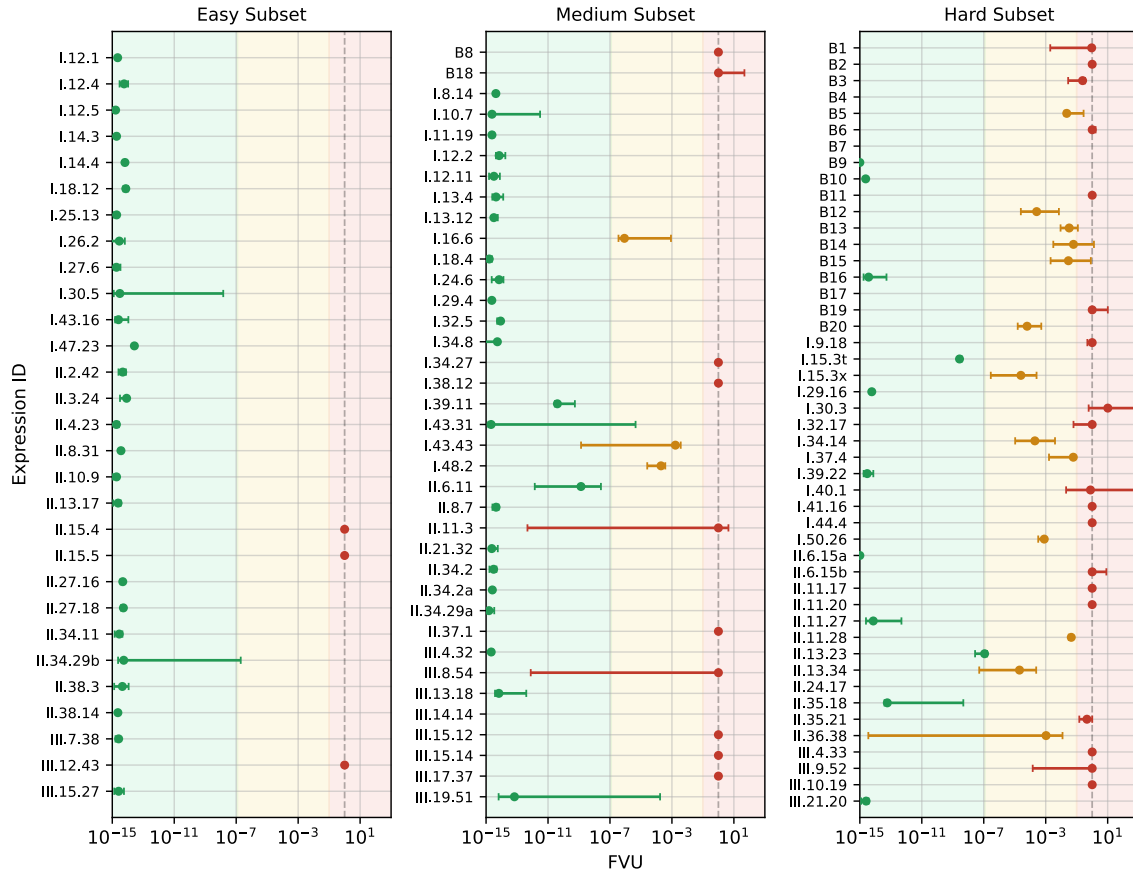


Figure 17. Median and 95% confidence intervals of the FVU with v23.0-120M, $\gamma = 0.05$, 8 optimizer restarts, 265k samples \approx 1000s across individual expressions in the FASTSRB benchmark stratified by difficulty level following (Matsubara et al., 2024). All but three “easy” expressions are solved perfectly (left, green dots). In both “medium” and “hard” categories, we observe a large number of approximate fits (orange) and failures (red) around $FVU \approx 0$ (gray dashed line) with increasing difficulty.

O. Token Embeddings

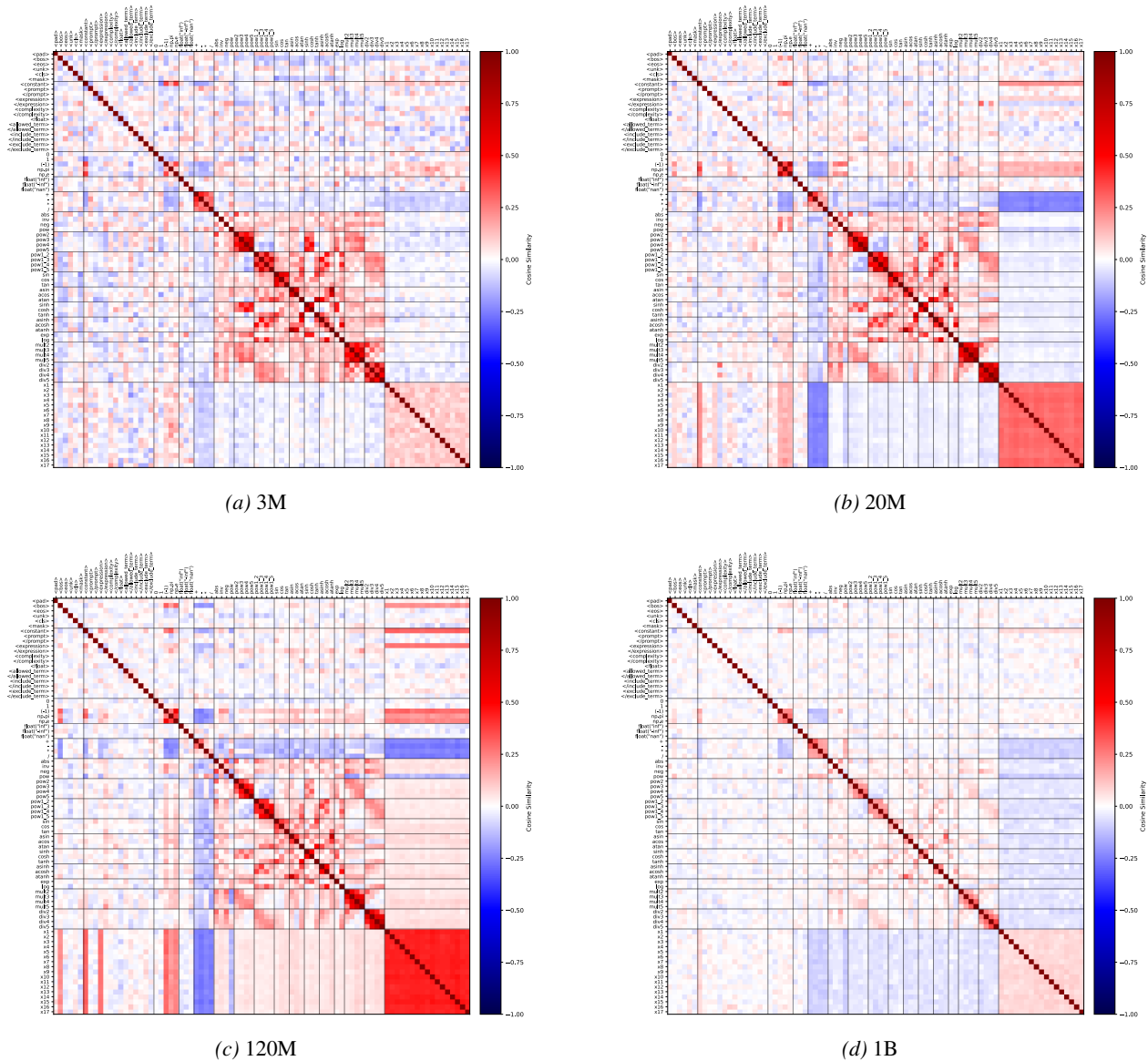


Figure 18. Token embeddings for the Flash-ANSR model family (v23.0) across model sizes. Across all scales, we observe high similarity of semantically related operators (e.g., binary operators, trigonometric functions, exponentials and powers) and variable tokens, and low similarity between different types of tokens (e.g. operators vs variables). The overall strength of these relationships varies across model sizes with no discernible pattern.